East European Journal of Physics. 2. 156-161 (2026)
DOI:10.26565/2312-4334-2026-2-15 ISSN 2312-4334

SYSTEMATIC CORRELATION BETWEEN SYNTHESIS PARAMETERS AND THE PARTICLE SIZE OF NICKEL OXIDE NANOCATALYSTS PREPARED BY THE SOL–GEL METHOD

Ilyos J. Abdisaidov*, Ilyos Kh. Khudaykulov, Usmonjon F. Berdiev, Sardor A. Tulaganov, Khatam B. Ashurov

Institute of Ion-Plasma and Laser Technologies named after U.A. Arifov, Academy of Sciences of the Republic of Uzbekistan, 100125, Durmon yuli st. 33, Tashkent, Uzbekistan
**Corresponding Author email: ilyos.abdisaidov@gmail.com*
Received September 8, 2025; revised April 4, 2026; accepted April 14, 2026

In this work, the sol-gel synthesis of nickel oxide (NiO) nanoparticles was systematically examined with respect to key parameters, including precursor type, reagent molar ratio, reaction time, and calcination temperature. A comparative evaluation of different nickel-based salts identified nickel nitrate as the most suitable precursor. Structural–phase characterization by X-ray diffraction (XRD) demonstrated that the nanoparticles synthesized at varying reagent ratios possessed well-defined crystalline phases, with an average crystallite size of ~11 nm. Prolonged reaction times were observed to promote agglomeration processes. Raman spectroscopic analysis revealed the presence of phonon and magnon vibrational modes, which were strongly dependent on particle size and calcination conditions. Transmission electron microscopy (TEM) confirmed a particle size distribution in the range of 3÷19 nm. Collectively, these results establish the synthesis–structure relationship and provide a framework for defining optimal conditions for preparing NiO nanocatalysts.
Keywords: *NiO nanocatalyst; Sol-gel method; Precursor type; Starting reagents; Reaction time; Calcination temperature*
PACS: 81,05 Rm; 61.46.Np

INTRODUCTION

The particle size and phase structure of NiO nanocatalysts are strongly dependent on the synthesis parameters. Among these parameters, the choice of precursor plays a decisive role, as it governs the crystallinity and morphology of the resulting nanoparticles. As reported in the scientific literature, nickel nitrate, nickel sulfate, and nickel chloride are the most commonly employed precursors [1–3]. Among them, nickel nitrate is highlighted as the most advantageous precursor due to its high solubility in water, low decomposition temperature, and the absence of residual by-products after the reaction. Furthermore, NiO thin films deposited via spray deposition using nickel nitrate as the precursor exhibit higher optical transmittance than films prepared with chloride and acetate precursors [4]. Therefore, in many studies, nickel nitrate is selected as the primary precursor.

The molar ratio of the starting reagents also has a pronounced impact on the efficiency of the synthesis process. For instance, an increase in the concentration of ammonium hydroxide decreases the average size of the resulting NiO nanoparticles, as OH^- ions passivate the particle surfaces, thereby reducing their propensity for agglomeration [5, 6]. This phenomenon has been experimentally confirmed in several studies, in which cation-anion interactions during hydrolysis have been identified as the primary governing factor [7]. Thus, optimizing the reagent ratio ensures the formation of uniformly distributed nanoparticles with reduced particle size.

Therefore, selecting an optimal reagent ratio is crucial for achieving the formation of uniformly distributed NiO nanoparticles with minimized particle size [8, 9]. This finding highlights the necessity of terminating the synthesis at an optimal time point.

Calcination temperature is likewise recognized as a key factor governing the particle size and degree of crystallinity of NiO nanoparticles. Literature reports indicate that calcination at relatively low temperatures (400–450 °C) can yield crystallite sizes of approximately 11÷12 nm [10, 11]. These results are corroborated by X-ray diffraction (XRD) and transmission electron microscopy (TEM) analyses, as well as by evidence of phase stability [12]. Conversely, increasing the calcination temperature can lead to particle coarsening and the emergence of additional phases within the crystalline structure.

For deeper characterization of the synthesized particles, Raman spectroscopy is widely employed to probe phonon and magnon excitations. In size-confined NiO nanoparticles, characteristic resonances - appearing at approximately ~500 cm^{-1}, ~730 cm^{-1}, and ~1090 cm^{-1} - are clearly manifested in the spectra [13]. These spectral signatures provide additional insight into the vacancy concentration and crystal symmetry of the synthesized nanoparticles.

In the sol–gel synthesis of NiO nanocatalysts, the choice of precursor, reagent stoichiometry, calcination time, and calcination temperature constitute the principal technological parameters [4,14]. Each exerts a pronounced influence on the morphology, particle-size distribution, and phase purity of the final product.

By judiciously optimizing these conditions, it is possible to obtain phase-stable, fine-sized NiO nanoparticles with high performance potential. This, in turn, provides a solid scientific basis for enhancing the efficiency of NiO-based

Cite as: I.J. Abdisaidov, I.Kh. Khudaykulov, U.F. Berdiev, S.A. Tulaganov, Kh.B. Ashurov, East Eur. J. Phys. 2, 156 (2026), https://doi.org/10.26565/2312-4334-2026-2-15
© I.J. Abdisaidov, I.Kh. Khudaykulov, U.F. Berdiev, S.A. Tulaganov, Kh.B. Ashurov, 2026; CC BY 4.0 license

catalysts across diverse application domains. In this article, the effects of these synthesis parameters on nickel oxide formation are examined in depth.

Parameters governing the size of NiO nanocatalysts

Nanocatalyst properties are dictated by synthesis conditions. In the sol–gel preparation of NiO, particle size is primarily controlled by precursor type, reagent stoichiometry, and reaction time. The following sections delineate the size–parameter relationships for each variable.

Precursor type.

In sol–gel routes to NiO nanoparticles, nickel nitrate, nickel sulfate, and nickel chloride are the predominant precursor salts used [15]. Among these precursors, nickel nitrate is advantageous owing to its high aqueous solubility and a substantially lower thermal decomposition temperature than nickel sulfate and nickel chloride. Using the aforementioned nickel-based salts as precursors, NiO nanoparticles were synthesized via a sol–gel route, and XRD was employed to assess crystallographic structure, phase purity, and phase composition; the corresponding diffraction patterns are presented in Figure 1.

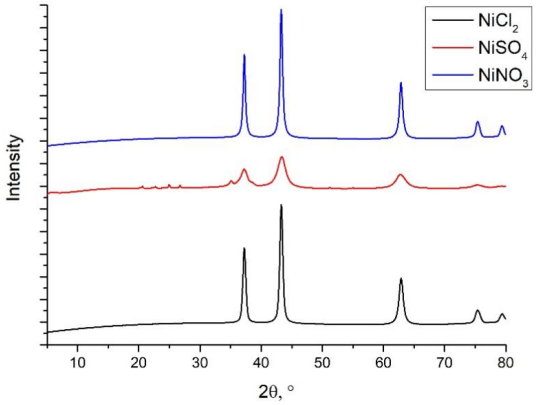

Figure 1. XRD patterns of NiO nanoparticles synthesized using different precursors

The diffraction patterns in Figure 1 were collected on a Rigaku SmartLab diffractometer using Cu Kα radiation (λ = 0.15405 nm) with a Kβ filter. Measurements were performed at 40 kV and 50 mA over a 2θ range of 5÷80°, with a scan rate of 3° min^{-1} and a constant step size of 0.01°, ensuring high-resolution, reliable data for subsequent analysis.

To ensure analytical fidelity, the 2θ step size was maintained at 0.01°, yielding a high-density dataset for subsequent analysis. All samples exhibit characteristic reflections of rock salt NiO at 2θ ≈ 37.2°, 43.3°, 62.8°, 75.3°, and 79.4°, indexed to the (111), (200), (220), (311), and (222) planes, respectively. The patterns obtained from nickel-nitrate-derived powders indicate superior crystallinity and phase purity, which is attributed to the cleaner decomposition of nickel nitrate and the absence of residual by-products - features not typically observed with nickel sulfate or nickel chloride. On this basis, nickel nitrate was selected as the precursor for subsequent sol-gel syntheses of NiO nanoparticles.

Effect of reagent stoichiometry on NiO nanocatalyst size.

The influence of starting-reagent stoichiometry on the size of sol-gel-derived NiO nanoparticles was investigated. Nickel nitrate and ammonium hydroxide were combined at varied molar ratios (n:m). Throughout the experiments, the amount of aqueous nickel nitrate was held constant, while the quantity of ammonium hydroxide was systematically increased to isolate the effect of base addition. The XRD patterns of the resulting powders are presented in Figure 2.

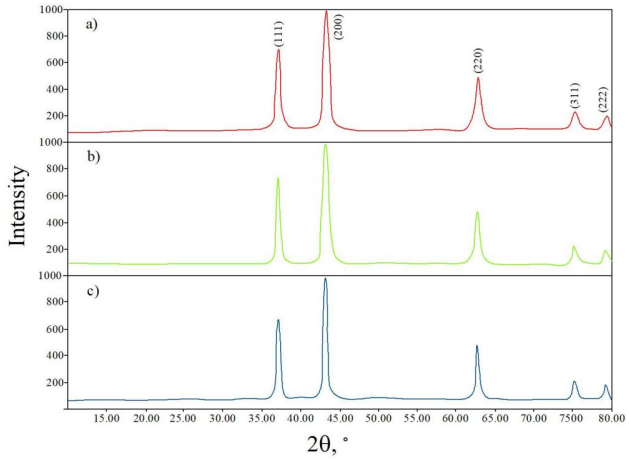

Figure 2. XRD patterns of NiO nanoparticles at reagent molar ratios: (a) 1:1; (b) 1:2; (c) 1:3

In Figure 2a, the aqueous solutions of ammonium hydroxide and nickel nitrate hexahydrate were used in equal amounts; in Figure 2b and Figure 2c, the amount of ammonium hydroxide was increased to 1:2 and 1:3 relative to the nickel nitrate hexahydrate solution, respectively. Across all three cases, the XRD diffractograms exhibit the characteristic reflections of rock salt NiO indexed to (111), (200), (220), (311), and (222) – at essentially identical 2θ positions, indicating that peak locations (and thus lattice symmetry) remain invariant with base-to-precursor ratio. The average crystallite size of the NiO powders was then estimated from the XRD peak broadening using the Debye-Scherrer equation [16].

$$D = \frac{K\lambda}{\beta cos\theta} \quad (1)$$

Here, K=0.9 is the Scherer's constant; λ is the X-ray wavelength (Cu-Kα); θ is the Bragg angle; and β is the full width at half maximum (FWHM) of the diffraction peak.

Figure 3 summarizes the dependence of NiO crystallite size on the starting-reagent molar ratio.

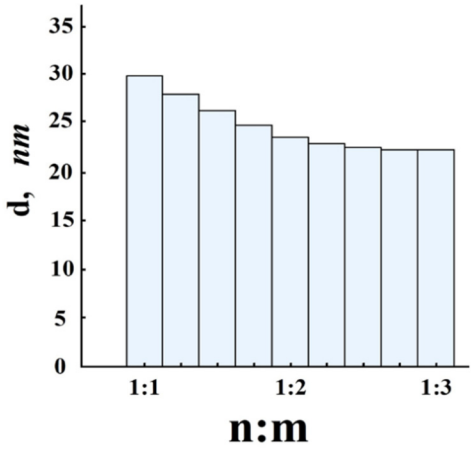

Figure 3. Dependence of NiO crystallite size on the starting-reagent molar ratio

From the histogram above, we conclude that as the amount of ammonium hydroxide increases during synthesis, the average size of the resulting NiO nanoparticles decreases. The reason is the passivation process: as the concentration of ammonium hydroxide increases, it alters the reaction medium, and the OH^- ions in ammonium hydroxide bind to the surfaces of the NiO nanoparticles, forming a complete shell that prevents agglomeration. As a result, the average size of the synthesized NiO nanoparticles decreases.

Dependence of the size of NiO nanocatalysts on reaction time

Another parameter influencing the synthesized NiO nanoparticles is the reaction time. The XRD results for NiO nanoparticles synthesized at different reaction times are shown below (Figure 4).

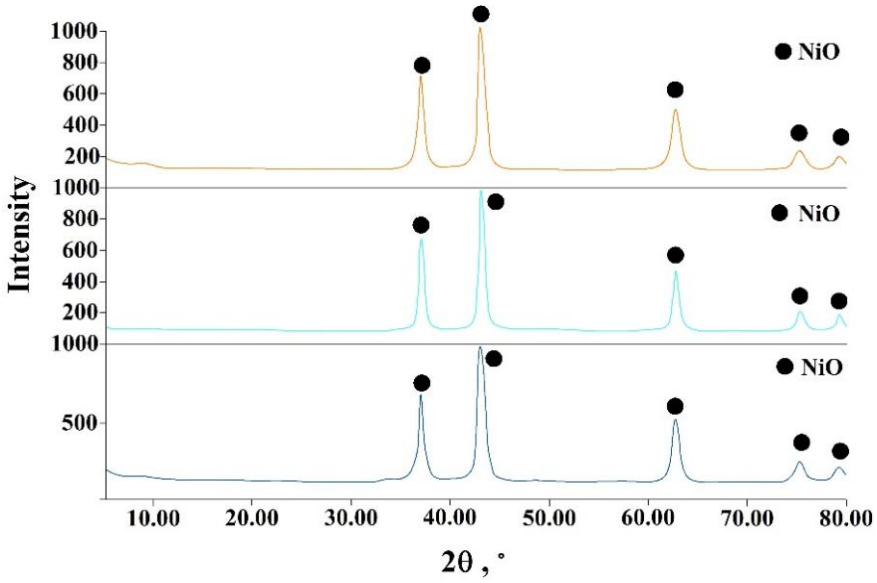

Figure 4. XRD patterns of NiO nanoparticles synthesized at different reaction times

In Figure 4 above, the XRD diffractograms of NiO synthesized by the sol–gel method at reaction times of 1 h, 2 h, and 3 h (from top to bottom) are presented. In all samples, the diffraction peaks corresponding to NiO(111), NiO(200), NiO(220), NiO(311), and NiO(222) are observed at diffraction angles 2θ ≈ 37.2°, 43.1°, 62.8°, 76.2°, and 79.3°, respectively. Using the XRD analysis results described above, the average crystallite size of the synthesized NiO nanoparticles was estimated according to equation (1). The effect of reaction time on particle size was investigated, and the results are summarized in the histogram shown below (Figure 5).

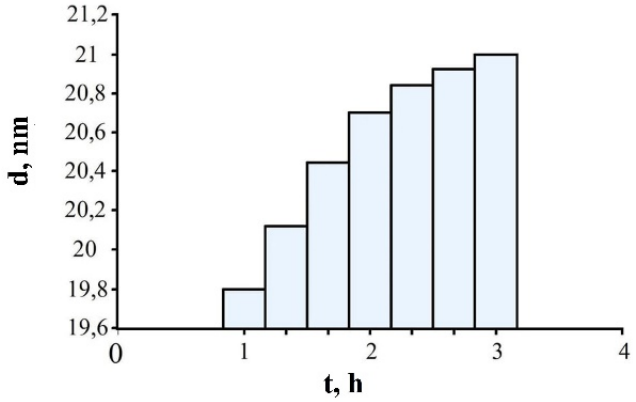

Figure 5. Dependence of NiO nanoparticle size on reaction time

As seen in Figure 5, no agglomeration was observed during the initial ~40 minutes of reaction. With further increases in reaction time, agglomeration of the NiO nanoparticles began gradually. This behavior is attributed to enhanced interparticle (atomic) collision forces that promote coalescence, resulting in a progressive increase in the particle size of the synthesized NiO nanoparticles.

EXPERIMENTAL PROCEDURE

Following a systematic evaluation of synthesis parameters, optimized conditions were adopted and the procedure was executed as follows: $Ni(NO_3)_2$ (7,25 g) was weighed as the nickel precursor and dissolved in deionized water (50 mL; Direct-Q 5UV) under magnetic stirring (MS7-H550-S) until a clear, homogeneous solution without visible precipitate was obtained. The resulting solution was then treated dropwise with 2 M NH_4OH (150 mL) while stirring continuously at 85 °C for 1 h. To ensure complete formation of nickel hydroxide, the mixture was aged at ambient temperature for 20 h. The pale-green suspension produced by the reaction was subjected to phase separation by centrifugation (EBA 20S) to isolate the solid fraction, assigned to $Ni(OH)_2$. The collected solid was calcined in a laboratory electric furnace (SNOL) at 400 °C for 2 h, then allowed to cool to room temperature, affording black NiO nanoparticles.

RESULTS AND DISCUSSION

The crystal structure, phase purity, and phase composition of NiO nanoparticles synthesized under optimal conditions were examined using the aforementioned diffractometer over a 2θ range of 5°÷80°, with a step size of 0.01°. The resulting XRD pattern is presented in Figure 6.

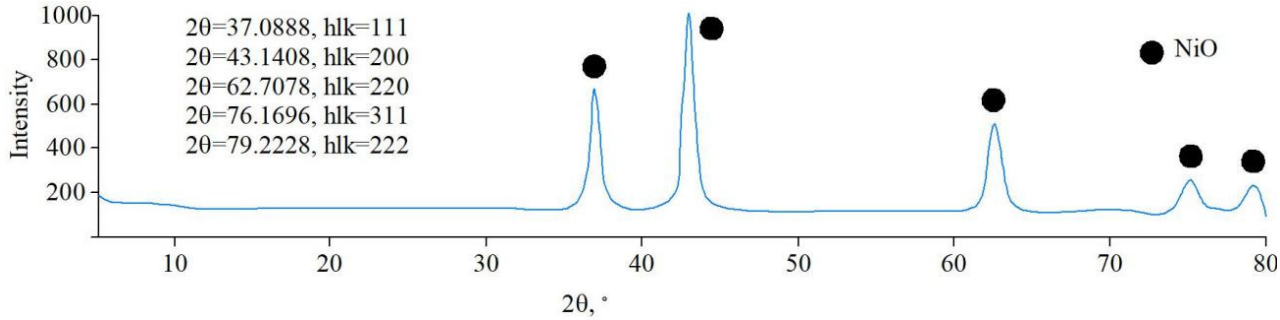

Figure 6. XRD pattern of NiO nanoparticles synthesized under optimized conditions

From Figure 6, reflections assigned to NiO(111), NiO(200), NiO(220), NiO(311), and NiO(222) are observed at diffraction angles 2θ = 37.08°, 43.14°, 62.70°, 76.16°, and 79.22°, respectively. The sharp, high-intensity peaks evidence a single-phase cubic NiO structure with lattice parameter a = 4.1901 Å, in good agreement with the Joint Committee on Powder Diffraction Standards (JCPDS) card No. 47-1049 [17]. The absence of additional satellite peaks in the XRD diffractogram indicates a high degree of phase purity in the synthesized NiO nanoparticles. Using equation (1), the average crystallite size was estimated to be ~11 nm. In other words, the low-temperature calcination employed here affords the most favorable outcome in terms of NiO crystallite size.

The Raman spectra of the synthesized NiO nanoparticles were recorded using Raman spectroscopy (RS) with 532 nm excitation (RL532, Class 3B laser). The spectra of the samples prepared under optimized conditions were examined by RS, and the resulting Raman profiles are presented (Figure 7).

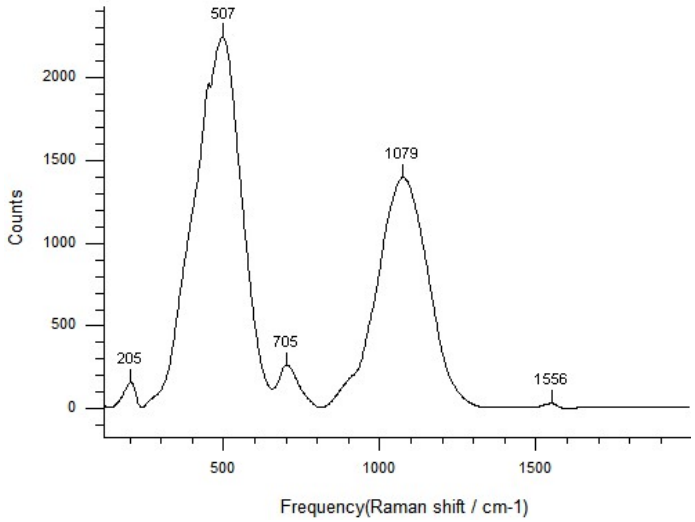

Figure 7. RS spectra of NiO nanoparticles synthesized under optimized conditions

As seen in Figure 7, a size and vacancy sensitive first-order phonon/magnon feature is observed at 507 cm^{-1}. The increased intensity of the Ni–O stretching mode at 507 cm^{-1}, the narrowing of the associated two-shoulder band, and the attenuation of the second-order phonon peaks at 705 cm^{-1} (transverse optical) and 1079 cm^{-1} (longitudinal optical) collectively indicate that the NiO nanoparticles synthesized under these conditions are of small characteristic size. A second-order magnon excitation is also evident at 1556 cm^{-1}. The clear appearance of the first-order transverse optical mode at 205 cm^{-1} further reflects the high sensitivity of the Raman setup employed.

To assess the particle size and morphology of the NiO nanoparticles synthesized under the above conditions, imaging was performed on a JEM-2100 Plus transmission electron microscope (TEM). A representative TEM micrograph is provided in Figure 8.

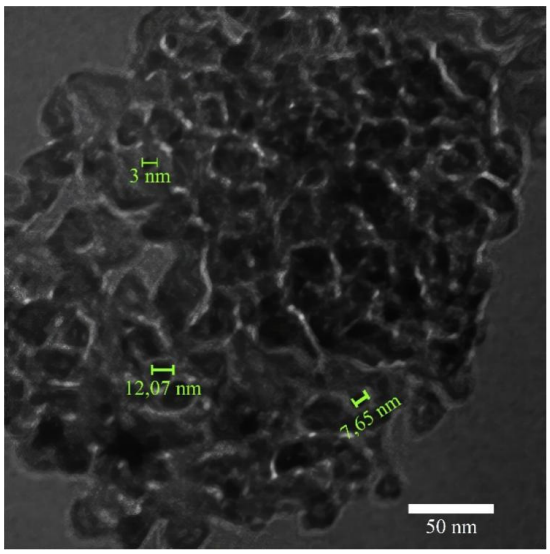

Figure 8. TEM micrograph of NiO nanoparticles synthesized under optimized conditions

From the TEM micrograph, the synthesized NiO nanoparticles exhibit a size distribution of 3÷19 nm. This is in close agreement with the average crystallite size estimated from the XRD data, confirming that the Scherrer-derived crystallite dimension is representative of the particle size.

CONCLUSIONS

The results demonstrate that, in the sol-gel synthesis of NiO nanoparticles, precursor type, reagent stoichiometry, and reaction time exert pronounced control over particle size and morphology. Nickel nitrate emerged as the optimal precursor owing to its high aqueous solubility and residue-free decomposition. A systematic increase in ammonium hydroxide content reduced the average particle size, consistent with hydroxide-driven surface passivation that suppresses

agglomeration. Conversely, extending the reaction time promoted particle coalescence. Under optimized conditions, the crystallite size was ~11 nm by XRD, in close agreement with TEM observations, thereby validating the structural uniformity of the product. Collectively, these findings provide a robust scientific and practical basis for the rational design and high-efficiency deployment of NiO-based nanocatalysts.

Acknowledgments

The authors gratefully acknowledge the financial and technical support provided by the Ministry of Higher Education, Science, and Innovation under project number IL-5421101842.

ORCID

Ilyos J. Abdisaidov, https://orcid.org/0000-0001-7473-1074; **Ilyos Kh. Khudaykulov,** https://orcid.org/0000-0002-2335-4456
Usmonjon F. Berdiev, https://orcid.org/0000-0003-2808-0105; **Khatam B. Ashurov,** https://orcid.org/0000-0002-7604-2333

REFERENCES

[1] A. Kistan, G. H. H. Priya, S. J. Raj, and L. Mayavan, Ionics, **31**(1), 1139 (2025). https://doi.org/10.21203/rs.3.rs-4985915/v1
[2] O.S. Makarenko and O.I. Hetman, Powder Metallurgy and Metal Ceramics, **62**(11), 633 (2024). https://doi.org/10.1007/s11106-024-00423-7
[3] M. Junaid, and M. Javed, Chemical Physics Impact, **3**, 100052 (2021). https://doi.org/10.1016/j.chphi.2021.100052
[4] M.M. Gomaa, G.R. Yazdi, S. Schmidt, M. Boshta, V. Khranovskyy, F. Eriksson, B.S. Faraga, *et al*., Materials Science in Semiconductor Processing, **64**, 32 (2017). https://doi.org/10.1016/j.mssp.2017.03.009
[5] M. Bonomo, Journal of Nanoparticle Research, **20**(8), 222 (2018). https://doi.org/10.1007/s11051-018-4327-y
[6] M.I. Din, R. Khalid, F. Arshad, Z. Hussain, and M. Batool, Inorganic and Nano-Metal Chemistry, **55**(6), 609 (2025). https://doi.org/10.1080/24701556.2024.2353768
[7] G.B. Veselov, T.M. Karnaukhov, V.O. Stoyanovskii, and A.A. Vedyagin, Nanomaterials, **12**(6), 952 (2022). https://doi.org/10.3390/nano12060952
[8] J. Mou, Y. Ren, J. Wang, C. Wang, Y. Zou, K. Lou, and D. Zhang, Microfluidics and Nanofluidics, **26**(4), 25 (2022). https://doi.org/10.1007/s10404-022-02534-2
[9] D. Pal, Indian Journal of Chemistry-Section A, **59**(10), 1513 (2020). https://nopr.niscpr.res.in/bitstream/123456789/55450/1/IJCA%2059A(10)%201513-1528.pdf
[10] A.M. Abd-Elnaiem, A. Hakamy, I.A. Ibrahem, A.M. Ali, W.A. Mohamed, and E.F.A. Zeid, Journal of Inorganic and Organometallic Polymers and Materials, **32**(6), 2209 (2022). https://doi.org/10.1007/s10904-022-02277-1
[11] L. Williams, A. R. Prasad, P. Sowmya, and A. Joseph, Materials Chemistry and Physics, **242**, 122469 (2020). https://doi.org/10.1016/j.matchemphys.2019.122469
[12] T.J. Wang, H. Huang, X.R. Wu, H.C. Yao, F.M. Li, P. Chen and Y. Chen, Nanoscale, **11**(42), 19783 (2019). https://doi.org/10.1039/C9NR06304H
[13] N. Mironova-Ulmane, A. Kuzmin, I. Sildos, L. Puust, and J. Grabis, Latvian Journal of Physics and Technical Sciences, **56**(2), 61 (2019). https://reference-global.com/download/article/10.2478/lpts-2019-0014.pdf
[14] Y. Wu, Y. He, T. Wu, T. Chen, W. Weng, and H. Wan. Materials Letters, **61**(14-15), 3174 (2007). https://doi.org/10.1016/j.matlet.2006.11.018
[15] S.S. Narender, V.V.S. Varma, C.S. Srikar, J. Ruchitha, P.A. Varma, and B.V.S. Praveen, Chemical Engineering & Technology, **45**(3), 397 (2022). https://doi.org/10.1002/ceat.202100442
[16] S. Fatimah, R. Ragadhita, D.F. Al Husaeni, and A.B.D. Nandiyanto, Asean Journal of Science and Engineering, **2**(1), 65 (2022). http://dx.doi.org/10. 17509/xxxxt.vxix
[17] A. Adiba, V. Pandey, S. Munjal, and T. Ahmad, AIP Conference Proceedings, **2270**(1), 110011 (2020). https://doi.org/10.1063/5.0020038

СИСТЕМАТИЧНА КОРЕЛЯЦІЯ МІЖ ПАРАМЕТРАМИ СИНТЕЗУ ТА РОЗМІРОМ ЧАСТИНОК НАНОКАТАЛІЗАТОРІВ ОКСИДУ НІКЕЛЮ, ВИГОТОВЛЕНИХ ЗОЛЬ-ГЕЛЬ МЕТОДОМ

Ільос Дж. Абдісаїдов, Ільос Х. Худайкулов, Усмонджон Ф. Бердієв, Сардор А. Тулаганов, Хатам Б. Ашуров
Інститут іонно-плазмових та лазерних технологій імені У.А. Аріфова Академії наук Республіки Узбекистан, 100125, вул. Дурмон йулі, 33, Ташкент, Узбекистан

У цій роботі систематично досліджували золь-гель-синтез наночастинок оксиду нікелю (NiO) з урахуванням ключових параметрів, зокрема типу прекурсора, молярного співвідношення реагентів, часу реакції та температури кальцинації. Порівняльна оцінка різних солей на основі нікелю визначила нітрат нікелю як найбільш підходящий прекурсор. Структурно-фазова характеристика за допомогою рентгенівської дифракції (XRD) показала, що наночастинки, синтезовані за різних співвідношень реагентів, мали чітко визначені кристалічні фази із середнім розміром кристалітів ~11 нм. Спостерігалися тривалі реакції, що сприяли процесам агломерації. Раманівський спектроскопічний аналіз виявив наявність фононних та магнонних коливальних мод, які сильно залежали від розміру частинок і умов кальцинації. Трансмісійна електронна мікроскопія (TEM) підтвердила розподіл розмірів частинок у діапазоні 3÷19 нм. У сукупності ці результати встановлюють взаємозв'язок між синтезом і структурою та забезпечують основу для визначення оптимальних умов приготування нанокаталізаторів NiO.

Ключові слова: *нанокаталізатор NiO; золь-гель метод; тип прекурсора; вихідні реагенти; час реакції; температура кальцинації*